ISSN 1063-7826, Semiconductors, 2018, Vol. 52, No. 2, pp. 254–259. © Pleiades Publishing, Ltd., 2018.
Original Russian Text © S.M. Pescherova, E.B. Yakimov, A.I. Nepomnyashchikh, L.A. Pavlova, O.V. Feklisova, R.V. Presnyakov, 2018, published in Fizika i Tekhnika Poluprovodnikov, 2018, Vol. 52, No. 2, pp. 266–271.

FABRICATION, TREATMENT, AND TESTING OF MATERIALS AND STRUCTURES

Electrical Activity of Extended Defects in Multicrystalline Silicon

S. M. Pescherova[a]*, E. B. Yakimov[b], A. I. Nepomnyashchikh[a], L. A. Pavlova[a], O. V. Feklisova[b], and R. V. Presnyakov[a]

[a] *Vinogradov Institute of Geochemistry, Siberian Branch, Russian Academy of Sciences, Irkutsk, 664033 Russia*
[b] *Institute of Microelectronics Technology and High Purity Materials, Russian Academy of Sciences, Chernogolovka, 142432 Russia*
** e-mail: spescherova@mail.ru*

Submitted February 9, 2017; accepted for publication February 16, 2017

Abstract—The excess carrier lifetime (τ) distribution in multicrystalline silicon grown by the Bridgman technique from high-purity metallurgical silicon (HPMG-Si) is studied. The features of the variation in τ, caused by the grain-boundary structure of ingots, are revealed. The grain boundaries, dislocations, and impurity microinclusions are studied by electron probe microanalysis (EPMA) and scanning electron microscopy (SEM) using selective acid etching. The electrical activity of extended defects is measured by the electron-beam-induced-current (EBIC) method.

DOI: 10.1134/S1063782618020124

1. INTRODUCTION

The main parameters of multicrystalline silicon (multisilicon) for solar-power engineering, used to estimate its quality, are the electrical characteristics (resistivity and excess carrier lifetime) and macrostructure parameters where an important role is played by the number of grain boundaries per unit ingot volume, their types, and crystallite orientation. It is supposed that columnar grain growth and large-grain structure formation occur in implementing planar crystal-melt interface conditions (Bridgman method). The electrical characteristics of multisilicon, which meet the requirements of solar-power engineering, can be achieved when using primary silicon with a base material part from 99.99 to 99.999 at %. In this case, the concentrations of impurities in the ingot will be at the level of their solubility limits in silicon and below [1]. The features of the production of multicrystalline silicon from high-purity metallurgical silicon (HPUMG-Si), we previously established, showed that violations in the columnar growth of silicon are associated with the transition to a concave crystal-melt interface [2]. This also leads to the formation of additional defects (dislocations, special boundaries, and others) which in turn affect the excess carrier lifetime distribution [3]. The electrical activity of special grain boundaries depends not only on the boundary structure, but also on the processes of impurity gettering at them and the reticular density of parent grains containing impurities [4–7]. The present paper is devoted to studying the interrelation of the electrical activity of extended defects with spatial distribution of the excess carrier lifetime.

2. MATERIALS AND EXPERIMENTAL

The objects of this study were multisilicon grains grown by the Bridgman method from upgraded metallurgical silicon (>99.99% purity grade). While maintaining identical conditions of Cr1, Cr2, Cr3, and Cr4 ingot crystallization (the crucible pulling and rotation rates are 0.5 cm/h and 1 rpm, respectively), the impurity contents in the primary metallurgical silicon were varied. The initial contents given in Table 1 were determined by inductively coupled plasma mass spectrometry (ICP-MS) [2].

The effective excess carrier lifetime in the multisilicon samples was measured using the Taumetr-2M setup by the contactless microwave-cavity method via the photoconductivity decay curve. Bulk photocarrier generation in the sample was excited by pulsed laser radiation with a wavelength of $\lambda = 1.06$ μm with the absorbance $\alpha \approx 10–15$ cm^{-1} in silicon. In the calculation of the bulk lifetime, we took into account the diffusion component of surface recombination. The effective excess carrier lifetime τ was measured according to the SEMI MF 1535 standard. In this case, the level of the start point in the decay curve was 0.7 of the photoconductivity signal; the end point level was $0.7/e$ of the photoconductivity signal. The conductivity type was determined via current rectification by the metal–semiconductor point contact; the electrical resistance was measured by the four-probe method using the Rometr setup.

At the bottoms and tops of each ingot (2 cm from the base and 2 cm from the top, respectively), plates $8 \times 6 \times 2$ mm in size were cut normally to the growth

Table 1. Concentrations (ppm) of major impurities in initial mixture compositions for growing multisilicon crystals

Ingot	B	P	Al	Ca	Mg	Ti	V	Cr	Mn	Fe	Co	Ni	Zr
Cr1	0.62	0.55	0.97	0.16	0.25	0.76	0.66	0.09	0.1	5.36	0.44	0.07	0.34
Cr2	0.21	0.18	0.32	0.05	0.08	0.26	0.22	0.03	0.03	1.79	0.15	0.02	0.11
Cr3	0.03	0.026	0.015	0.008	0.012	0.036	0.031	0.004	0.005	0.26	0.021	0.003	0.016
Cr4	0.21	0.18	0.45	0.24	0.3	0.38	0.3	0.014	0.04	6.12	0.17	0.1	0.12

Table 2. Electrical parameters of multisilicon ingots, measured along the growth axis in height *F* from the ingot bottom edge

F, cm		0.5	0.15	0.25	0.35	0.45	0.55	0.65	0.75	0.85	0.95	Average value
Cr1	ρ, Ω cm	0.23	0.22	0.22	0.22	0.22	0.26	0.23	0.19	0.18	0.17	0.21
	τ, μs	2.53	2.06	2	2.23	2.03	2.2	2.6	1.93	1.93	2.03	2.15
Cr2	ρ, Ω cm	0.67	0.66	0.66	0.65	0.63	0.6	0.56	0.53	0.5	0.46	0.59
	τ, μs	3.1	2.7	3.5	3.4	3.2	3.1	2.4	2.4	2.3	3.1	2.92
Cr3	ρ, Ω cm	1.6	1.7	1.8	1.8	1.73	1.67	1.62	1.79	2.25	2.61	1.85
	τ, μs	3.8	3.7	3.5	4	5.3	44	19.3	12.9	9.26	6.73	11.25
Cr4	ρ, Ω cm	0.8	0.77	0.72	0.7	0.68	0.66	0.64	0.62	0.6	0.55	0.67
	τ, μs	1.17	0.8	0.9	1.17	0.96	0.92	0.93	0.73	1.15	1.12	0.98

axis. These plates were used to measure the excess current lifetime in sequentially arranged sample surface areas 2 × 2 mm in size, comparable to the light spot diameter of 2 mm. To determine the recombination rate of excess carriers by the EBIC method, the samples were chemically polished in a HF and HNO_3 acid solution, and then Al was deposited to create Schottky barriers; ohmic contacts were formed on the underside by rubbing with Al–Ga paste. After measuring the induced current, the deposited layer was removed in HF:H_2O solution; then the sample surface was mechanically polished followed by the use of selective Dash etchant (HF:HNO_3:CH_3COOH) for studying the sample surface structure using a JEOL JXA8200 microanalyzer in the scanning electron microscope (SEM) mode.

3. RESULTS AND DISCUSSION

Along the growth axis, over the entire ingot height (10.5 cm), the electrical parameters such as the conductivity type, the resistance ρ, and the excess carrier lifetime τ were determined. The Cr1, Cr2, and Cr4 crystals had *p*-type conductivity; the Cr3 crystal had *n*-type conductivity. The data obtained are given in Table 2.

As seen in Table 2, the distributions of the resistance and excess carriers τ in the ingots differ appreciably: ρ gradually varies over the height of all crystals under study, whereas τ undergoes drastic changes. This is especially noticeable in the Cr3 sample where the highest averaged values of ρ and τ are observed. Among other crystals, the highest values of ρ and τ are observed in Cr4 and Cr2, respectively. Of particular interest were the factors responsible for the behavior of the distribution of τ in the crystals. Therefore, further measurements over the surface of samples cut from the bottom (B) and top (T) of each ingot were performed. Figure 1 shows a schematic representation of the measurement regions of excess carriers τ on the surface of samples Cr1, Cr2, Cr3, and Cr4.

For further studies, samples Cr2(T) and Cr3(T) with a higher excess carrier value τ were chosen. Moreover, anomalously high excess carrier values τ (26.5 and 9 μs) were measured in two adjacent Cr3(T) sample areas (Fig. 1). To determine the interrelations between the parameters τ and the multisilicon macrostructure, the surface was studied using SEM. Figure 2 shows SEM images of the Cr2(T) and Cr3(T) sample surface, composed of fragments obtained by backscattered electrons (BEI) which we enumerated in the matrix form.

As seen in Fig. 2, the macrostructure of the samples under study is significantly different. For Cr2(T), as for the entire ingot, the fine-grained structure with straight boundaries parallel to each other is characteristic (Fig. 2a), whereas Cr3 (Fig. 2b) exhibits a large-grain columnar structure with bent boundaries. Figure 2 shows that the sample surfaces are divided into sectors each corresponding to a certain excess-carrier value τ (μs). The highest excess-carrier values τ in Cr2(T) (see Fig. 1b) correspond to sectors 1/1 (1.35 μs), 2/1 (2 μs), 3/1 (1.4 μs), 4/1 (1.8 μs) with coarse-grained structures and minimum numbers of bent boundaries (sectors 2/1 and 3/1 contain subgrains with twin boundaries). In Cr3(T), the high values of τ correspond to sectors 1/3 (7.1 μs), 2/3 (8 μs), 4/1 (9 μs), and 4/2 (26.5 μs) containing grain bound-

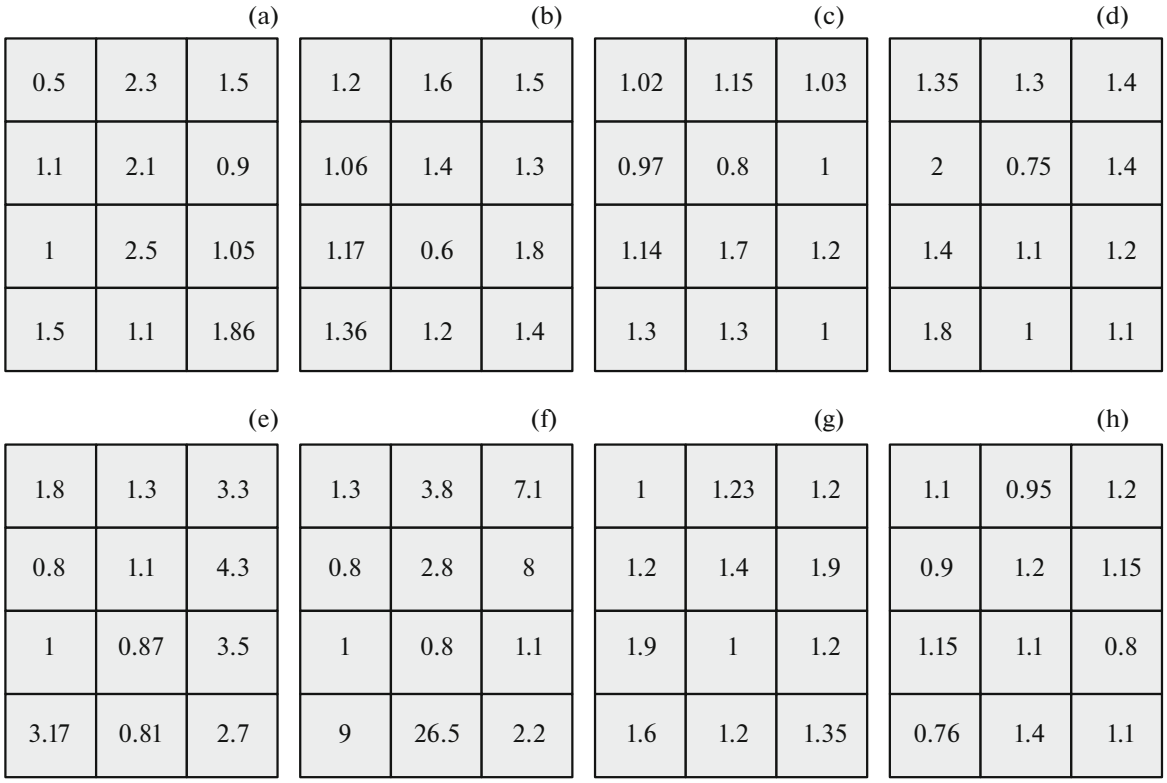

Fig. 1. Excess-carrier distribution maps τ (in μs) over the sample surface perpendicular to the multisilicon ingot growth axis. Samples: (a) Cr1(B), (b) Cr1(T), (c) Cr2(B), (d) Cr2(T), (e) Cr3(B), (f) Cr3(T), (g) Cr4(B), (h) Cr4(T).

aries, whereas boundaries are lacking in sectors with the least values of τ (sectors 3/2 and 3/3). To determine the major causes of the decrease in parameter τ, the spatial distribution of the electrical activity over the whole surface area of samples Cr2(T) and Cr3(T) was studied. Then, samples were subjected to selective chemical etching to detect the fine surface structure and electrically active defects. The results obtained are shown in Fig. 3.

The grain boundary from sector 1/1, as seen in Figs. 3a and 3e, is electrically active; after etching, it represents a convex line along which microinclusions (*1–3* in Fig. 3a) and etch pits are arranged. In this case, etch pits are equiprobably observed in the boundary plane and in the grain, whereas microinclusions are mostly arranged along the boundary line. In sector 2/1, microinclusions are electrically active defects and exist both at the boundary (*4* in Fig. 3b) and in the grain (*5* in Fig. 3b). The band of dislocation etch pits in sector 3/2 exhibits pronounced electrical activity and contains microinclusions (*6* in Figs. 3c and 3g). Despite the electrical activity partially or wholly exhibited by boundaries in sector 4/1, the value of τ in this sector is high in comparison with sectors 1/1, 2/1, and 3/2. The highest EBIC contrast in this sector is exhibited by special boundaries with increased contents of etch pits in comparison with nearby grain regions (Figs. 3d and 3h). The compositions of microinclusions *1–8* in Fig. 3 are given in Table 3.

Almost all microinclusions are electrically active, independently of their position. The characteristic features are a small size (no more than 0.5 μm in diameter) and spherical shape. It is more probable that all these objects are secondary-type microinclusions; they are formed in the boundary crystalline multisilicon layer, being localized at extended microstructural

Table 3. Elemental composition of points indicated in Fig. 3 as microinclusions in Cr3(T)

No.	Si	O	C	Al	Na	Mg	Ca	Cr	Cu	Zn
1	100.0	n.d.	n.d.	n.d.	<0.1	n.d.	n.d.	n.d.	n.d.	n.d.
2	99.9	n.d.	n.d.	<0.1	n.d.	<0.1	n.d.	n.d.	n.d.	n.d.
3	99.9	n.d.	n.d.	n.d.	<0.1	<0.1	n.d.	n.d.	n.d.	n.d.
4	85.8	13.1	n.d.	1.082	n.d.	n.d.	n.d.	n.d.	n.d.	n.d.
5	59.4	29.2	n.d.	n.d.	n.d.	n.d.	11.4	n.d.	n.d.	n.d.
6	20.6	22.7	23.3	n.d.	n.d.	n.d.	n.d.	33.4	n.d.	n.d.
7	n.d.	n.d.	n.d.	n.d.	n.d.	n.d.	n.d.	n.d.	60.5	39.5
8	99.9	n.d.	n.d.	n.d.	<0.1	n.d.	n.d.	n.d.	n.d.	n.d.

No. is the microinclusion number. The composition was determined using a JXA8200 microanalyzer and a JEOL EX-84055MU energy-dispersive spectrometer. The content of elements is given in wt %; n.d. means not detected.

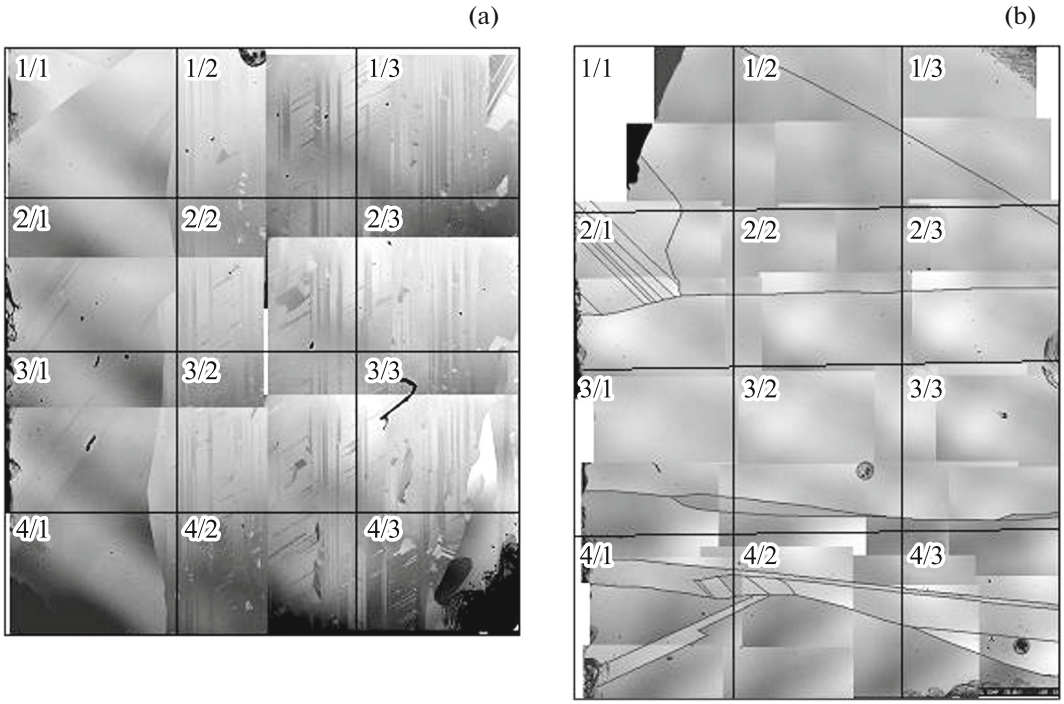

Fig. 2. SEM images of the polished sample surface, composed of backscattered-electron (BEI) fragments: (a) Cr2(T), magnification is ×60; (b) Cr3(T), magnification is ×40.

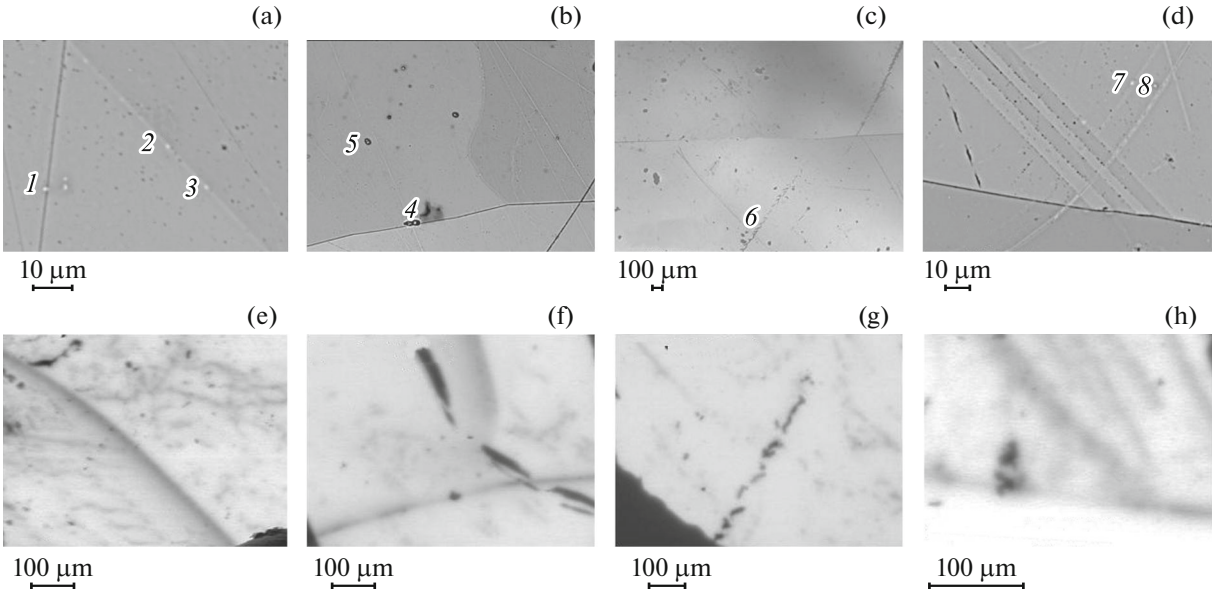

Fig. 3. Sector images: (a, b, c, d) SEM (BEI) images of etched surfaces of Cr3(T) sector fragments 1/1, 2/1, 3/2, and 4/1, respectively (*1*–*8* are microinclusion); (e, f, g, h) EBIC images of sector fragments 1/1, 2/1, 2/2, and 4/1.

defects (dislocations, grain boundaries). For example, microinclusions *2*, *3*, *4* (Figs. 3a and 3b) are arranged at grain boundaries and locally enhance their electrical activity, thus significantly decreasing the average τ in a given sector. Microinclusions *1*, *5*, *7*, and *8* (Fig. 3a, 3b, 3d) arranged in grain regions in combination with structural defects (characteristic of dislocations judging by etch pits) have no less effect on excess-carrier value τ than microinclusions at grain boundaries.

Figure 3h shows the Cr3(T) 4/1 sector fragment with twin boundaries along which there are many dis-

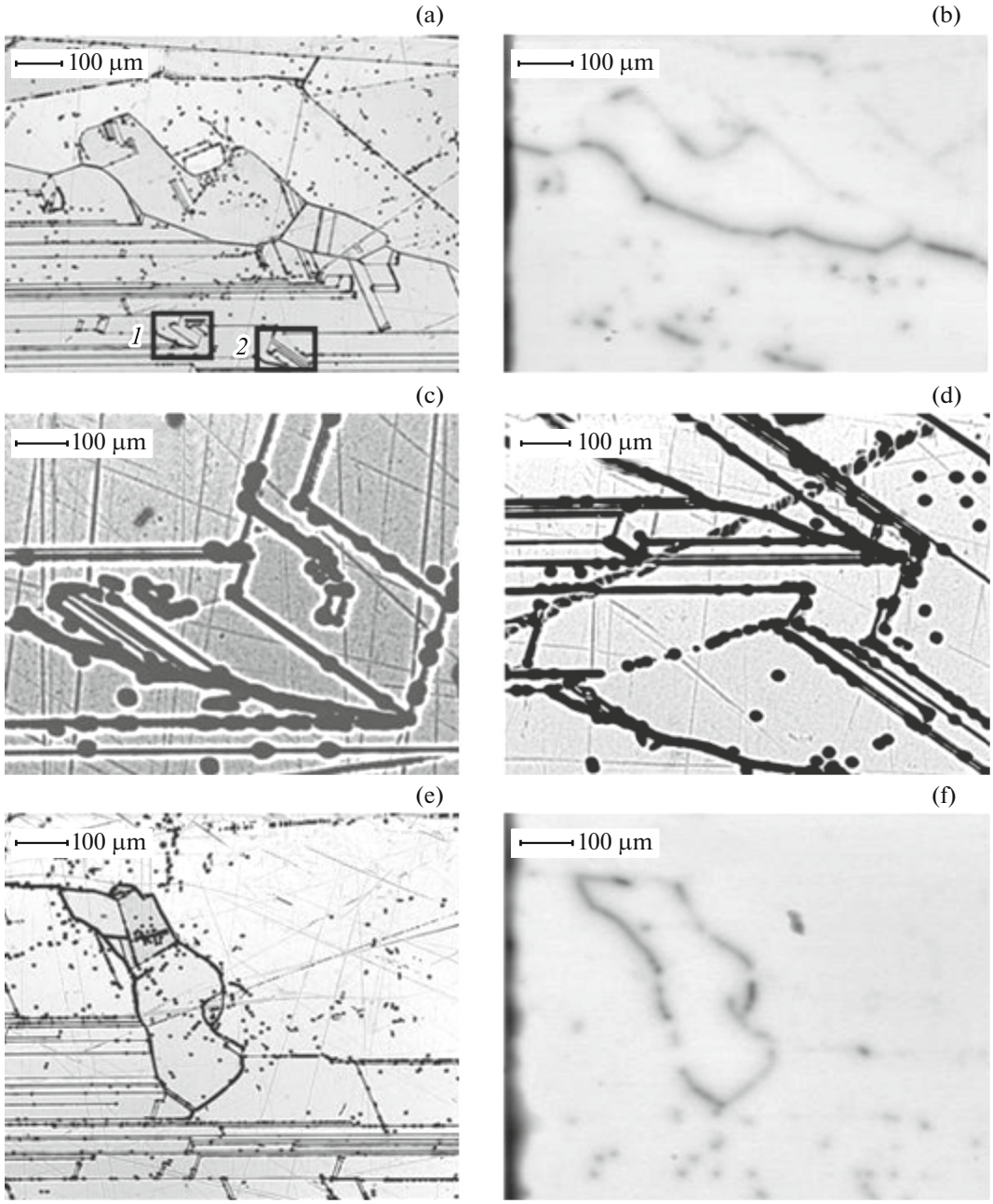

Fig. 4. (a) SEM image (BEI) of the etched surface of the Cr2(T) sector fragment 1/3; (b) EBIC image of the surface of the Cr2(T) 1/3 sector; (c, d) SEM images of the etched surface of fragments *1* and *2* separated in panel (a), respectively; (e) SEM image (BEI) of the etched surface of the Cr2(T) 2/3 sector; (f) EBIC image of the surface of the Cr2(T) 2/3 sector.

location etch pits. These boundaries exhibit much lower electrical activity, and τ in this sector is ten times higher than in sectors 2/1 and 3/2. This is probably due to the lack of microinclusions in the grain boundary region.

Of interest is the fact the initial impurity content in the Cr3 mixture (except for Al, see Table 1) is lower than in Cr2 by a factor of (6.7 ± 0.7). In this case, Cr3 has *n*-type conductivity in contrast to other crystals. It should be noted that the unified etching conditions had a different effect on the surface state of the Cr2(T) and Cr3(T) samples: microinclusions were not detected on the Cr2 sample surface (Fig. 4).

As seen from the results of the EBIC study of the Cr2(T) surface, only a small fraction of grain boundaries is electrically active (Figs. 4b and 4f). If we consider that the images of these fragments contain many grain boundaries, electrical activity is exhibited only by boundaries of a certain shape (with bent profiles

and a high content of etch pits; their structure also distinctly differs from neighboring electrically inactive boundaries. Bent boundaries are boundaries with random orientation, and their contrast is always stronger than the contrast of special boundaries.

4. CONCLUSIONS

The results of studying the spatial distribution of the recombination activity of grain boundaries and extended defects in multisilicon, showed that the optimum electrical properties of a given material cannot be achieved proceeding from only macrostructure parameters such as the density of grain boundaries per unit ingot volume or crystallite orientation. An important role in macro- and microstructure formation is played by impurities existing in primary metallurgical silicon. Depending on their concentration and ratio of elements, microinclusions of certain types and compositions are formed. It was found that secondary microinclusions have a significant effect on the recombination activity of structural defects (dislocations, grain boundaries) and are mostly responsible for a decrease in bulk electrical characteristics than defects with a higher distribution density without microinclusions.

ACKNOWLEDGMENTS

This study was supported by the Russian Foundation for Basic Research (project no. 16-35-00140-mol_a) using scientific equipment of the Shared Service Center of the Isotopic–Geochemical Research of the Institute of Geochemistry, Siberian Branch, Russian Academy of Sciences, Irkutsk.

REFERENCES

1. B. G. Gribov and K. V. Zinov'ev, Inorg. Mater. **39**, 653 (2003).
2. A. I. Nepomnyashchikh, R. V. Presnyakov, I. A. Eliseev, and Yu. V. Sokol'nikova, Tech. Phys. Lett. **37**, 739 (2011).
3. S. M. Peshcherova, A. I. Nepomnyashchikh, L. A. Pavlova, I. A. Eliseev, and R. V. Presnyakov, Semiconductors **48**, 476 (2014).
4. S. M. Peshcherova, A. I. Nepomnyashchikh, and L. A. Pavlova, Tech. Phys. Lett. **40**, 1000 (2014).
5. S. M. Peshcherova, E. B. Yakimov, A. I. Nepomnyashchikh, L. A. Pavlova, and O. V. Feklisova, Semiconductors **49**, 724 (2015).
6. S. Tsurekawa, K. Kido, and T. Watanabe, Mater. Sci. Eng. A **462**, 61 (2007).
7. J. Chen, T. Sekiguchi, D. Yang, F. Yin, K. Kido, and S. Tsurekawa, J. Appl. Phys. **96**, 5490 (2004).

Translated by A. Kazantsev